ELSEVIER

European Journal of Mechanics B/Fluids 21 (2002) 429–446

EUROPEAN JOURNAL OF MECHANICS B/FLUIDS

Active control of the turbulent flow over a swept fence

André Huppertz, Hans-Hermann Fernholz *

Hermann-Föttinger-Institut für Strömungsmechanik, Technische Universität Berlin, 10623 Berlin, Germany

Received 3 July 2001; accepted 1 March 2002

Abstract

The aim of this experimental investigation has been to reduce the length of the three-dimensional separation region downstream of a swept surface-mounted fence by time-periodic blowing and suction generated by loudspeakers along a spanwise slot either upstream of or at the tip of a fence. The sweep angles were 0° and 20° and the Reynolds number $\mathrm{Re}_h \equiv U_N h/\nu = 5330$.

Two flow phenomena were used for the manipulation of the shear layer and the reduction of the separation length:

- the coherent structures of the separated shear layer (Kelvin–Helmholtz instability) were influenced to increase entrainment by single and bimodal forcing at the tip of the fence. Here the effective disturbance amplitude could be small (e.g., $A = O(0.1U_N)$);
- the corner flow upstream of the fence was manipulated by the upstream actuator-slot so that a starting-type vortex roll formed at the tip of the fence, increased entrainment just downstream of the fence and reduced the separation length. Here the effective disturbance amplitude was large (e.g., $A = O(U_N)$).

Reattachment could be reduced at most by about 35% of the non-manipulated reattachment length. Measurements in the flow field were performed by LDA and DPIV and on the wall by pulsed-wire anemometry (PWA).

Keywords: Separated turbulent flow; Fence flow; Time-periodic forcing; Experimental study; Optimal forcing frequency; Vortex dynamics; Control of mean reattachment length

1. Introduction

The flow over a surface-mounted sharp-edged fence with a height of the order of the boundary layer contains two strong perturbations (Bradshaw and Wong [1]): the upstream and the downstream separation bubble, the latter interacting with the shear layer separating from the sharp edge. Both the upstream separation bubble and the shear layer are susceptible to disturbances and can thus be used to reduce the reattachment length of the downstream separation bubble. This determines the locations of a possible manipulation of the flow and disturbances can be introduced either upstream of the front separation line or directly into the shear layer at the tip of the fence. If the fence is swept in downstream direction, the separation region becomes shorter than when it is straight but the disturbance mechanisms remain generally the same. The size of the sweep angle generally affects, however, the three-dimensional behavior of the downstream bubble. For sweep angles smaller than 30° the three-dimensional separation region remains spanwise invariant over about 60% of the span.

Siller and Fernholz [2] – henceforth denoted SF – and Siller [3] investigated the flow over an unswept straight fence with and without manipulation. Here the actuators were located upstream of the front separation line and oriented parallel to the

* Correspondence and reprints.
E-mail address: fernholz@pi.tu-berlin.de (H.-H. Fernholz).

0997-7546/02/$ – see front matter
PII: S0997-7546(02)01190-1

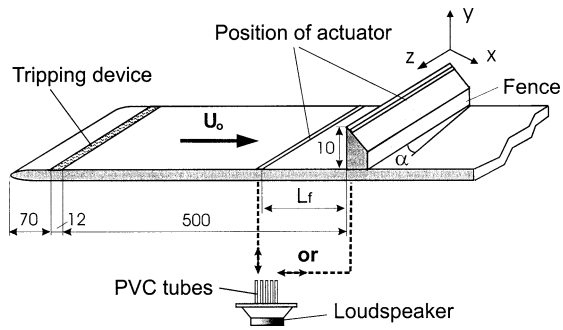

Fig. 1. Schematic view of the test plate, the fence and the locations of the actuator (coordinate system: x is perpendicular and z is parallel to the fence).

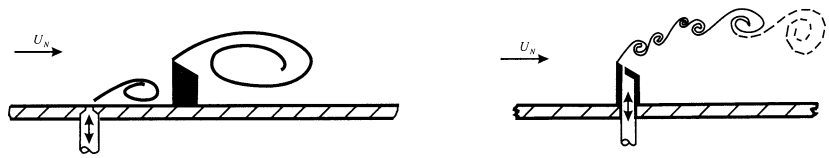

Fig. 2. Different excitation locations and its effects on the flow viewed in the x, y-plane.

fence. They consisted either of a spoiler with movement normal to the wall or a two-dimensional oscillating jet with zero mass flow driven by loudspeakers. With appropriate tuning of the flow parameters the reattachment length downstream of the straight fence could be reduced by 50% with a forcing amplitude of $v'/U_N \approx 210\%$ (for a definition see Section 3).

The present experiment extends the SF investigation in two ways in that a fence is used with a sweep angle of $\alpha = 20^\circ$ and the two-dimensional oscillating jet is situated at the top of the fence (TF) or upstream of the fence (UF) (Fig. 1). Depending on the frequency and the amplitude of the disturbance, the manipulation of the flow at either of the two locations has a significant effect on the length of the reattachment region downstream of the fence but the mechanisms involved are different (Fig. 2).

If the actuator is located upstream of the separation region in front of the fence (Siller [3]), the periodic roll-up of the spanwise vortex changes the flow upstream of the fence dynamically so that the shear layer separating from the fence moves in a flapping motion. This generates a large vortex immediately downstream of the fence which increases the entrainment into the bubble and thus reduces the reattachment length. This can be achieved only by a large amplitude $A = v'/U_N$ with an order of 100%. If the actuator is at the tip of the fence, the optimum amplitude can be smaller but the optimum frequency increases from $\mathrm{St}_h \equiv fh/U_N = 0.05$ to about 0.125. The reduction of the reattachment length begins also at much smaller amplitudes ($A \approx 10\%$) since the disturbance influences the Kelvin–Helmholtz instability of the separated shear layer. It should be noted that the Kelvin–Helmholtz instability neither scales with the fence height nor with the reattachment length.

There are several experimental and numerical investigations of flows over straight and swept backward-facing steps with and without manipulation. For a more detailed list of references we refer to Huppertz [4] and mention only investigations which have a closer relationship with the present experiment (Hasan [5], Fernholz et al. [6], Chun and Sung [7], Huppertz and Janke [8], Kaltenbach and Janke [9] and Wengle et al. [10]).

There are, however, hardly any experiments on flows over a swept fence. Related investigations were performed by Hancock and Mc Cluskey [11] and by Hardman and Hancock [12,13] in the flow downstream of a vertical flat plate swept at different angles to the main flow and mounted on the front of a horizontal splitter plate. No flow control was applied.

In the following we shall describe briefly the experimental set-up and the measuring techniques, show features of the undisturbed flow field and then present the two mechanisms of manipulation and their effects on the separation region downstream of the fence.

2. Experimental set-up and measuring techniques

The experiments were performed in an open-circuit suction-type wind tunnel at the Hermann-Föttinger-Institute of the Technical University of Berlin (Schober [14]). The contraction ratio of the nozzle was 9.0 and the settling chamber was equipped with a filter mat and a perforated metal plate (open area ratio 64%) as a grid. This arrangement provided very uniform flow conditions in the test section (Dengel [15]). The test section had a cross-section of 500 mm × 500 mm and a length of 1500 mm. The top and the side walls of the test section were made of flint glass to allow access for Laser-Doppler and PIV measurements

and flow visualisations. The test section was followed by a rectangular duct leading to the centrifugal blower. The model (Fig. 1) was fixed in the inlet of the test section. It consisted of a plate with an elliptical nose and the surface-mounted fence. The fence of height $h = 10$ mm was located 570 mm downstream of the leading edge, where the top of the fence was chamfered at an angle of 30°. The aspect ratio was $B/h = 50$ and the blockage was $h/H = 2.4\%$. The centre-plane of the plate was 110 mm above the lower side of the nozzle exit so that the nozzle boundary layer was removed from the test section. In order to obtain well defined starting conditions for the test boundary layer the stagnation point was fixed at the upper side of the elliptical nose with a perforated metal plate at the outlet of the test section providing the necessary flow resistance. A Velcro tape (height 3.5 mm) 70 mm downstream of the leading edge ensured transition so that the fence was approached by a fully turbulent boundary layer.

The bulk of the experiments was conducted at a free-stream velocity component normal to the fence $U_N \equiv U_\infty \cos(\alpha) =$ 8 m/s. The free-stream turbulence intensity in the test section was 0.2%.

The forcing device consisted of chamber with a slot (width $b = 1.2$ mm) connected via PVC tubes of equal length (diameter 10 mm, length 500 mm) to six loudspeakers. This ensured that the phase of the perturbation at the outlet did not vary along the slot. The loudspeakers were driven by power amplifiers, and a computer with a 12 bit D/A converter served as a signal generator. The forcing slot was located either in the test plate upstream of the fence or at the tip of the fence.

The *velocity measurements* were conducted using a commercial two-component LDA (Dantec fiber flow optics/burst spectrum analyser 57N10) or a PIV system (PCO Computer Optics/Optical Flow Systems). The LDA was operated in the continuous mode measuring coincident velocities only. The sampling time was 30 seconds and a typical burst rate in the shear layer 1.2 kHz. The spatial resolution of the measuring volume was $(\Delta x, \Delta y, \Delta z) = (0.15, 0.15, 2.35)$ mm. The LDA was mainly used for single profile measurements whereas the PIV was applied to capture the large scale vortex dynamics. The PIV equipment consisted of a CONTINUUM 25 mJ Nd:YAG Laser and a CCD cross-correlation camera (PCO SENSI CAM with a resolution of 1024×1280 pixels). The data were processed by the OFS software VIDPIV 4.0. The interrogation spots had a size of 32×32 pixels and an overlap of 75%. Outliers of the cross correlation were identified by the detectability criterion ($k = 1.2$) of Kean and Adrian [16]. The spatial resolution was $(\Delta x, \Delta y, \Delta z) = (2, 2, 2)$ mm. The mean velocities measured by LDA agreed well with the PIV data, therefore the inaccuracy of the mean values is estimated less than 4%. However, the Reynolds stresses were measured more precisely with LDA because the spatial resolution was 10 times smaller than for the PIV system. The uncertainty of these values is estimated to be less than 10%.

Skin friction was measured using pulsed-wire anemometry (e.g., Fernholz et al. [17]). According to [17] the error of this technique can be estimated as ±4%.

The *wall streamlines* of the reverse-flow region were visualized by a suspension of petroleum and TiO_2 or by silicone oil droplets. With this technique, the location of the reattachment line could be determined within an uncertainty of ±5 mm, i.e., $\pm 0.5h$.

Mean *wall pressure* was measured by a high sensitive capacitance pressure transducer (MKS Baratron 120 AD) and the *pressure fluctuation* above the forcing slot by a B&K 2669 microphone and a B&K amplifier.

3. Flow parameters and flow conditions upstream of the fence

The emphasis of this investigation was on the manipulation of the flow over a straight and a swept surface mounted fence in a turbulent boundary layer, using two locations for the excitation and maintaining the same boundary conditions. The aim was to reduce the mean reattachment length $\bar{x}_R$ which – made dimensionless by the fence height h – depends on the following quantities:

$$\frac{\bar{x}_R}{h} = f\Bigg(\underbrace{\underbrace{\frac{\delta_o}{h}, \frac{U_N h}{\nu}, \frac{B}{h}, \frac{H}{h}, \alpha, T_{u_\delta}}_{\text{without manipulation}}, \frac{f_i h}{U_N}, \frac{v_i'}{U_N}, \frac{\lambda_z}{h}, \frac{d}{h}, \frac{b}{h}}_{\text{with manipulation}}\Bigg).$$

Here δ_0 denotes the boundary layer thickness at separation, U_N the free-stream velocity normal to the fence, B the width of the test section, H the height of the test section, α the sweep angle, T_{u_δ} the free-stream turbulence level, ν the kinematic viscosity, f_i and v_i' the frequency and the peak amplitude of each perturbation wave (Fourier decomposition), λ_z the spanwise wave length of the disturbance, d the distance between the fence and the upstream actuator and b the slot width which was constant.

Siller [3] performed a rather extensive study of the parameters affecting the flow over a surface mounted straight fence and we have based the choice of most parameters on his results. He found, for example, that Reynolds number effects do not play a role for $\mathrm{Re}_h \geqslant 4000$. This was also confirmed for the swept case (see Fig. 3) and so Re_h was chosen as 5330. The blockage was reduced to $h/H = 2.4\%$ and the aspect ratio was increased to $B/h = 50$. In accordance with Hancock and Mc Cluskey [11]

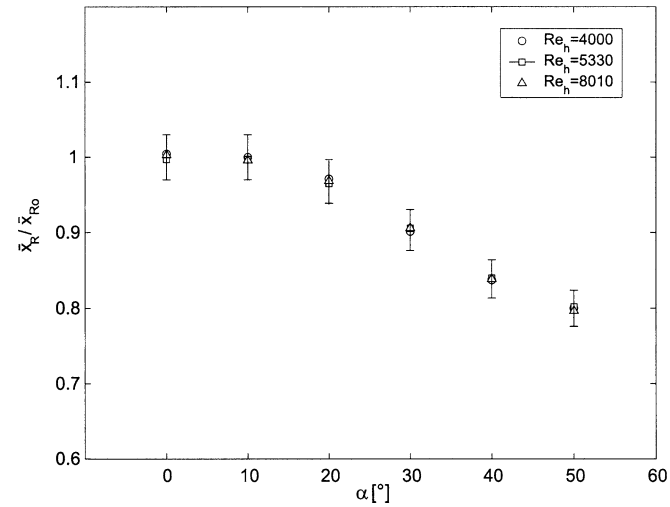

Fig. 3. Mean reattachment length as a function of the sweep angle α for different Reynolds numbers Re_h ($\bar{x}_{R0}/h = 15.5$).

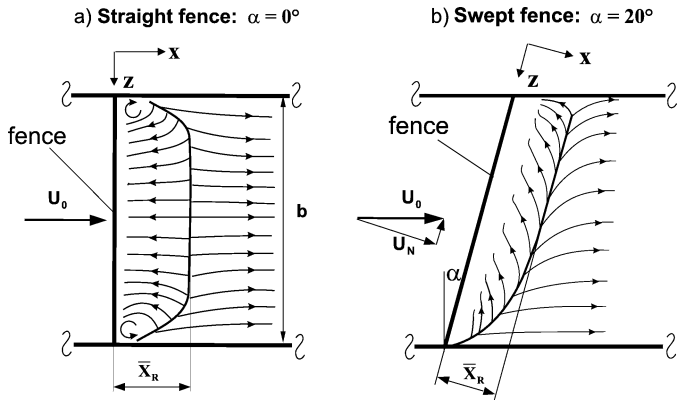

Fig. 4. Wall streamlines downstream of a straight or a swept surface mounted fence. View from above.

this was necessary to ensure a spanwise-invariant flow over a relevant region parallel to the fence. The length of this region was strongly dependent on the sweep angle. Fig. 4 shows the wall streamlines for sweep angles $\alpha = 0°$ and 20° determined from flow visualizations by means of a suspension of TiO_2 and petroleum and with droplets of silicone oil.

The distribution of $\bar{x}_R/h$ in spanwise direction z/h shows the extent of the spanwise invariance as a function of the sweep angle α (Fig. 5). Spanwise-invariance at the wall does not imply self-similar behavior of the mean and fluctuating velocity profiles. Our experiments (not shown here) show that the profiles are self-similar at different positions z/h for $\alpha = 20°$ in a range at least $z/h \leqslant 10$. For $\alpha = 50°$, although $\bar{x}_R/h$ is spanwise invariant over a larger distance than for $\alpha = 20°$, the flow field is inhomogeneous and measurements would have had to be performed at each station x and z. This is the reason why these data could not be measured in the time available. It should be mentioned here that the reattachment point is defined by $\bar{\tau}_{wx} = \mu(\partial\bar{u}/\partial y)_{y=0} = 0$ whereas the component $\bar{\tau}_{wz} = \mu(\partial\overline{w}/\partial y)_{y=0}$ is different from zero in all cases with a sweep angle.

The flat plate on which the fence was mounted had an elliptical leading edge parallel to the unswept fence. This configuration was also used when the fence was swept for the simple reason that the spanwise skin friction distribution measured at $x = 535$ mm varied only by ±2% over the center region. For a swept leading edge this variation (not shown here) was larger and the distribution revealed a rather wavy pattern in spanwise direction which was due to longitudinal vortices caused by cross-flow instabilities (Bippes [18]) and which was undesirable for the downstream development of the flow. So we preferred a variable distance between the leading edge and the fence to a small variation in the boundary layer thickness. Without the fence in place – the mean velocity distribution and the Reynolds stresses were measured 500 mm downstream of the tripping device at the position of the fence. The mean velocity profile was typical of that in a canonical boundary layer ($\mathrm{Re}_{\delta_2} = 1050$, $H_{12} = 1.43$) and the Reynolds stresses agreed well with Spalart's DNS data (Spalart [19]). So the flow upstream of the fence was a 2D turbulent boundary layer (see Fig. 6) with a ratio of boundary layer thickness over fence height of about two ($\delta_{99}/h \approx 2$).

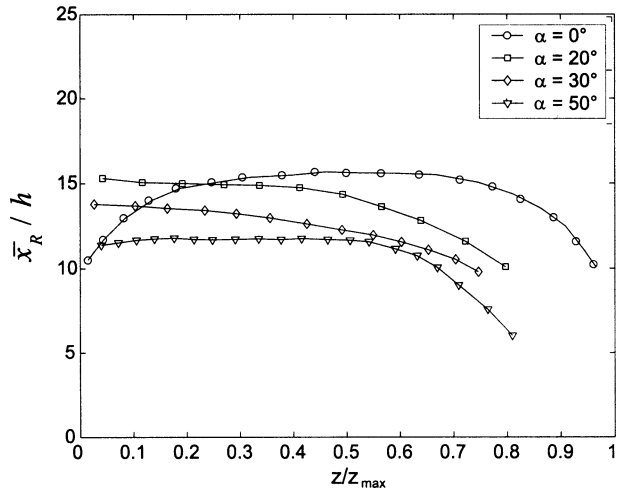

Fig. 5. Rettachment length downstream of the fence in spanwise direction for different sweep angles α ($B/h = 50$, $\delta_{99}/h \approx 2$, $\mathrm{Re}_h = 5330$).

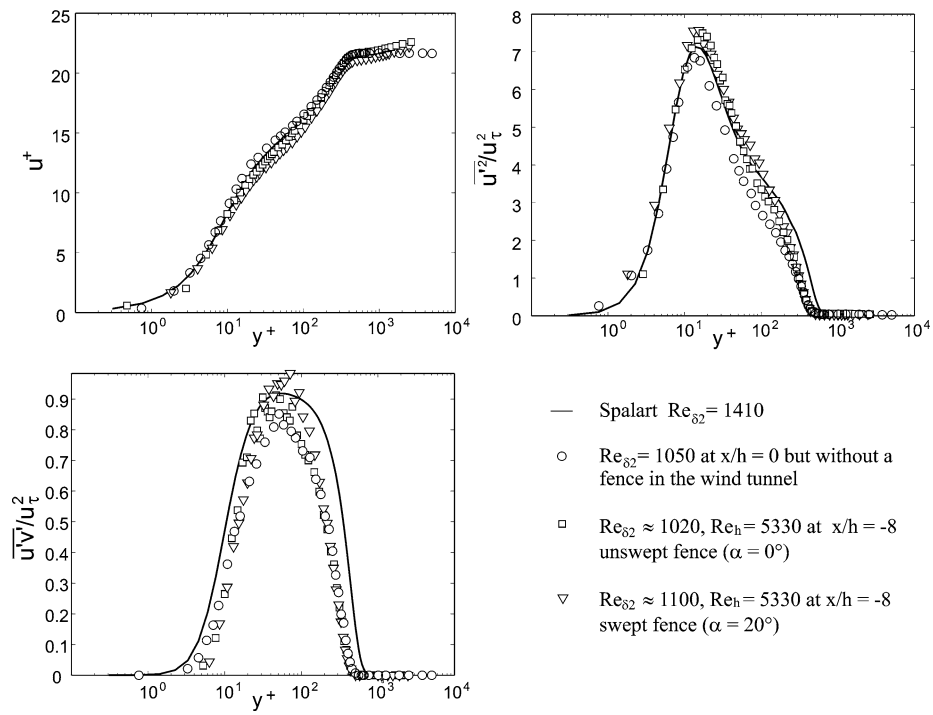

Fig. 6. Boundary layer profiles: (○) at location of the fence ($x/h = 0$) without a fence in place; (□) upstream ($x/h = -8$) of the unswept fence ($\alpha = 0°$); and (▽) upstream ($x/h = -8$) of the swept fence ($\alpha = 20°$).

4. Optimization of the excitation parameters and reduction of the reattachment length

As was mentioned above, the flow over the fence was manipulated by an oscillating two-dimensional jet flow (zero net mass flux) from a spanwise slot situated either upstream of the fence or at the tip of the fence. The optimum location of the upstream slot was parallel to the fence and upstream of the separation line. The slot distance from the fence l_f was found to have an optimum between 1.5 and 2h and l_f/h was chosen as 1.5 in agreement with Siller [3]. The peak amplitudes of the disturbances $\langle v \rangle_{\max}$ were measured above the slot at the position of the maximum value by phase-averaged LDA measurements of the v'-component. Fig. 7(a) shows the v'-component as a function of time above the slot and Fig. 7(b) the pressure fluctuations

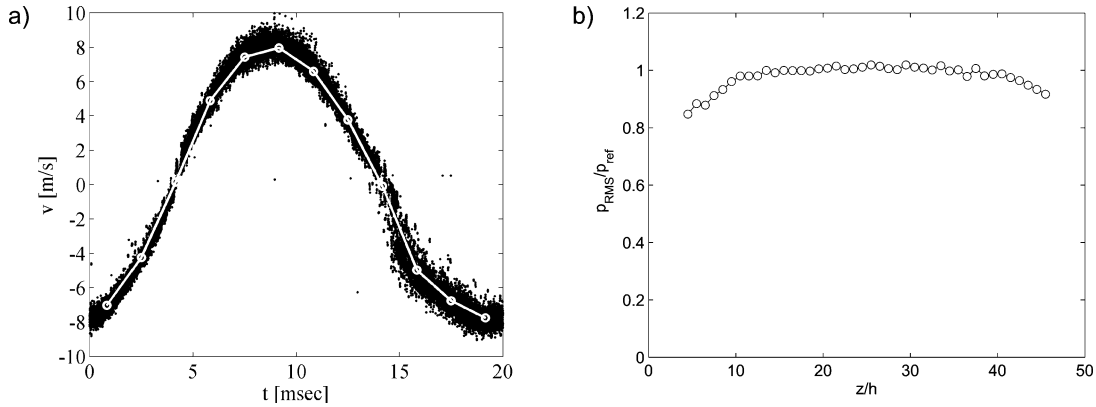

Fig. 7. (a) v-component above the slot and (b) pressure intensities along the slot ($A \equiv \langle v \rangle_{\max}/U_N = 100\%$, $f = 50$ Hz).

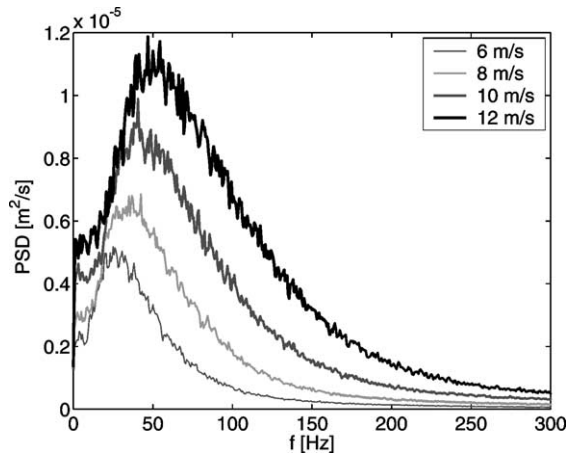

Fig. 8. Power spectral density distribution at various freestream velocities U_N at $(x/h, y/h = (10, 3.8))$ (no manipulation).

above the slot in spanwise direction 25 mm above the slot for $f = 50$ Hz measured by a microphone. Here the peak amplitude of v' had the same order of magnitude as the velocity of the oncoming flow and its distribution was sinusoidal.

Large-scale quasi-periodical vortical structures of the separated shear layers play a key role in flow control. These coherent structures are caused by a stochastic roll-up process due to the inflectional velocity profiles. On average there are, however, preferred frequencies, which show as a bump in the power spectral density of the streamwise velocity fluctuation and shift to higher frequencies with increasing mean velocity (Fig. 8). The frequencies of these amplified waves have been shown earlier to be effective excitation frequencies. They were therefore measured at the outer edge of the undisturbed shear layer ($x/h = 10$, $y/h = 3.8$) at the x position of the maximum integral turbulence production (see below) and were found to be linearly related to the freestream velocity component U_N. The Strouhal number $\mathrm{St} = fL/U$ could then be formed using U_N, $f = f_{\mathrm{bump}}$, and a characteristic length L which could be the fence height, the momentum loss thickness δ_2 or the reattachment length $\bar{x}_R$. Since the effects of the manipulations upstream of (UF) or at the tip of the fence (TF) affect different flow phenomena the most effective Strouhal numbers must be determined for each case separately.

Flow manipulation at the tip of the fence with low amplitudes affects the Kelvin–Helmholtz instability of the shear layer. Here the appropriate local Strouhal number is $\mathrm{St}_{\delta_2} = f\delta_2/\bar{u}_{\max}$, where $\delta_2(x)$ is the momentum loss thickness of the separated shear layer

$$\delta_2 = \int_{y_a}^{y_b} \frac{\bar{u}}{\bar{u}_e}\left(1 - \frac{\bar{u}}{\bar{u}_e}\right) \mathrm{d}y \quad \text{with} \quad y_a = y(\bar{u} = \bar{u}_{\min}), \qquad y_b = y\big(\overline{u'v'} = 0\big) \quad \text{and} \quad \bar{u}_e = \bar{u}\big(\overline{u'v'} = 0\big)$$

and $\bar{u}_{\max}(x) \approx \bar{u}_e(x)$ the maximum velocity of the profile. Mean and fluctuating velocity profiles at $x_2/h = 10$ were measured for upstream velocities between $U_N = 6$ and 12 m/s and, when scaled by $\bar{u}_{\max}$ and h, fell on top of each other (not shown).

In this case δ_2 and $\mathrm{St}_{\delta_2} = 0.020$ remain constant. The same holds for the respective Strouhal numbers $\mathrm{St}_h = 0.045$ and $\mathrm{St}_{\bar{x}_R} = 0.61$. St_{δ_2} can now be used to calculate an optimum excitation frequency close to the fence at $x_1/h = 1$, according to the relationship

$$f(x_1) = f(x_2)\frac{\delta_2(x_2)}{\delta_2(x_1)}\frac{\bar{u}_{\max}(x_1)}{\bar{u}_{\max}(x_2)}.$$

With all other parameters having been constant, this gave $f_1 = 114$ Hz which is close to the optimum frequency for case TF (see Fig. 10(a) below). The orientation of the spanwise vortices was determined by cross correlation between two hot wires displaced in spanwise direction. It was found to be normal to the outer flow velocity U_0 and not parallel to the swept fence, similar to the spanwise vortices downstream of a swept step (Kaltenbach and Janke [9]). Since the reduction of the reattachment length was not affected by this small "misalignment" the wave fronts of the excitation were generated parallel to the fence.

4.1. Single frequency forcing

Figs. 9 and 10 show the effect of the manipulation at the excitation locations UF and TF on the mean reattachment length $\bar{x}_R$, made dimensionless by the non-manipulated length $\bar{x}_{R0}$, for sweep angles 0° and 20°. For variable frequency the

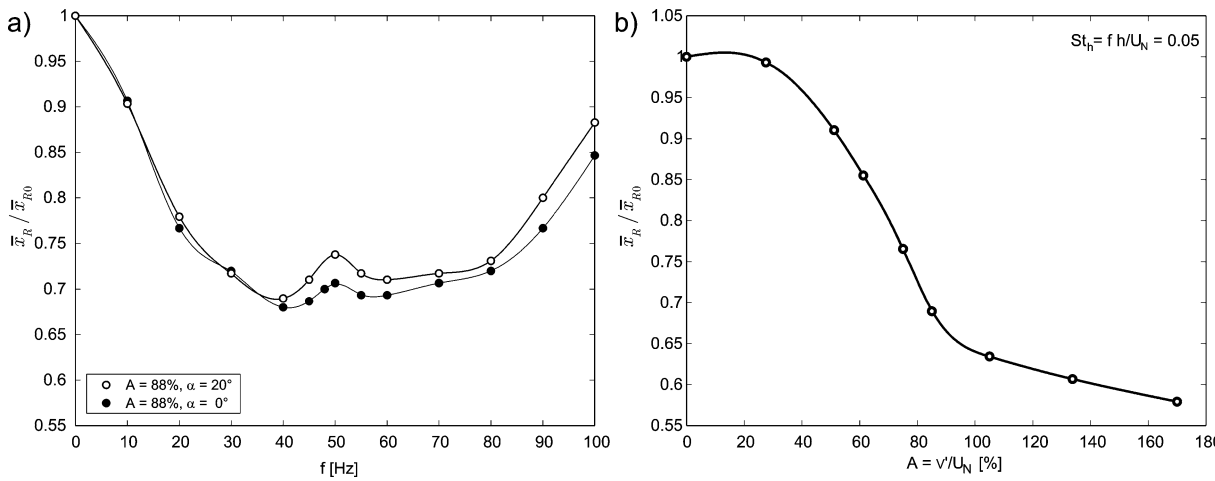

Fig. 9. Non-dimensional reattachment length for the excitation upstream of the fence (a) as a function of the excitation frequency and the sweep angle α and (b) as a function of the excitation amplitude ($\mathrm{St}_h = 0.05$, $f = 40$ Hz, $\alpha = 20°$).

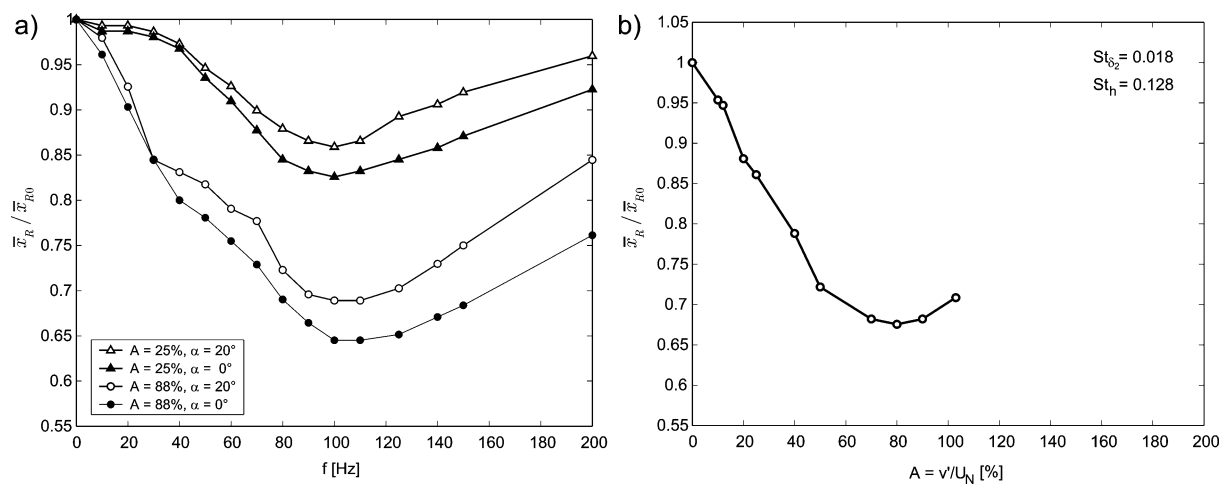

Fig. 10. Non-dimensional reattachment length for the excitation at the tip of the fence (a) as a function of the excitation frequency and the sweep angle α and (b) as a function of the excitation amplitude ($\mathrm{St}_{\delta_2} = 0.018$, $f = 102$ Hz, $\alpha = 20°$).

amplitude was fixed at $A = 25\%$ and 88%, respectively. The choice of the amplitude values $A = \langle v \rangle_{\max}/U_N$ will be explained subsequently.

Fig. 9(a) shows the development of $\bar{x}_R/\bar{x}_{R0}$ for case UF as a function of the excitation frequency f and the sweep angle α at a fixed amplitude $A = 88\%$. The minimum value $\bar{x}_R/\bar{x}_{R0}$ lies at an optimum excitation frequency $f_{\text{opt}} = 40$ Hz and is practically independent of α. The corresponding Strouhal number St_h is 0.05 and for this value and a sweep angle of 20° the dimensionless reattachment length $\bar{x}_R/\bar{x}_{R0}$ was measured as a function of the amplitude A at the slot (Fig. 9(b)). For values of A below 35% the reattachment length does not change. For larger values of the amplitude $\bar{x}_R/\bar{x}_{R0}$ falls to 0.66 at $A = 88\%$ from where the slope changes to a smaller gradient.

For the excitation at the tip the development of $\bar{x}_R/\bar{x}_{R0}$ was measured as a function of the excitation frequency, two values of the amplitude A and of the sweep angles α (Fig. 10(a)). The optimum excitation frequency is approximately 100 Hz, independent of sweep angle and amplitude. This value is slightly below the most unstable frequency of the shear layer calculated above (see also Wengle et al. [10]). For an amplitude of 88% the reattachment length is reduced over the whole frequency range below 100 Hz. This is not the case for $A = 25\%$ where a lower limit of the frequency of about 20 Hz must be exceeded before an effect occurs. It should be noted in contrast to case UF that a reduction is achieved for low values of A if the optimum excitation frequency is used (Fig. 10(b)). It will be shown later that it is the Kelvin–Helmholtz instability mechanisms which is the cause for the increased entrainment and the reduced reattachment length. The optimum Strouhal numbers are $\text{St}_h = 0.128$ and $\text{St}_{\delta_2} = 0.018$, with δ_2 determined at the location $x/h = 1$ (without reverse flow). The development of the reattachment length as a function of the amplitude A shows a minimum at about $A = 80\%$.

The excitation of the Kelvin–Helmholtz instability at $f_{\text{opt}} = 102$ Hz can be explained (Ho and Huerre [20]) by the behaviour of the kinetic energy of the coherent structures $\overline{u'^2}_{\text{coh}}$ integrated over the width of the shear layer E_{coh}:

$$E_{\text{coh}}(u; f_0) = \int_0^{\infty} \frac{\overline{u'^2}_{\text{coh}}(f_0)}{U_N^2}\,\mathrm{d}(y/h) \quad \text{with} \quad \overline{u'^2}_{\text{coh}}(f_0) = \int_{f_0-\Delta f}^{f_0+\Delta f} S_{uu}(f)\,\mathrm{d}f,$$

where S_{uu} is the power spectral density of the u' fluctuation (note that: $\overline{u'^2} = \int_0^{\infty} S_{uu}(f)\,\mathrm{d}f$), $[\Delta f - f_0, \Delta f + f_0]$ is the spectral bandwidth of the coherent energy and f_0 is the excitation frequency f_{exc} or the corresponding subharmonic ($f_{\text{sub}} = \frac{1}{2} f_{\text{exc}}$). Here the coherent energy of the u' fluctuation was measured by a single hot wire in the region with no reverse flow because the sampling rate of the LDA system was not high enough. No subharmonic component of f_{exc} could be detected in the frequency spectrum of the shear layer, i.e., no vortex pairing occurred (Ho and Huang [21]). Hence the coherent energy was only calculated for the excitation frequency.

Fig. 11 shows the profiles of $\bar{u}$ and $\overline{u'^2}$ of the unforced and forced case ($f = 102$ Hz, $A = 25\%$) in the vicinity of the fence at $x/h = 1$. Forcing did not change the mean velocity profile and the total fluctuation energy is also unaffected. This means for the forced case that only a small part of the stochastic fluctuation has been transformed into the coherent mode. Compared to the total fluctuation energy, the coherent part is very small, i.e., the effective forcing amplitude is small.

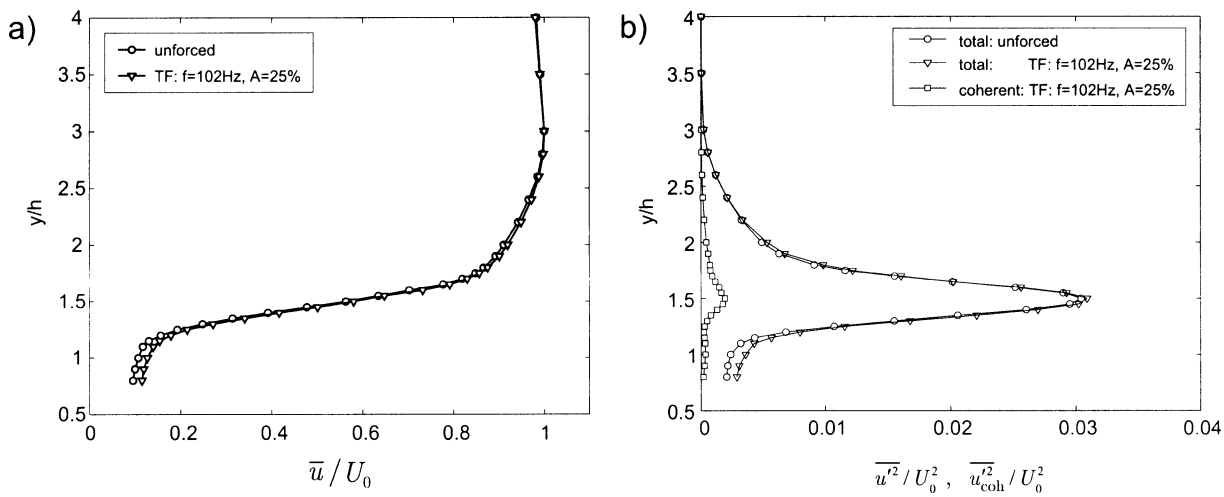

Fig. 11. Profiles of the mean velocity $\bar{u}/U_N$ (a) and of the Reynolds normal-stress $\overline{u'^2}/U_N$ (b) at $x/h = 1$ for the unforced and the forced case (TF: $f = 102$ Hz, $A = 25\%$).

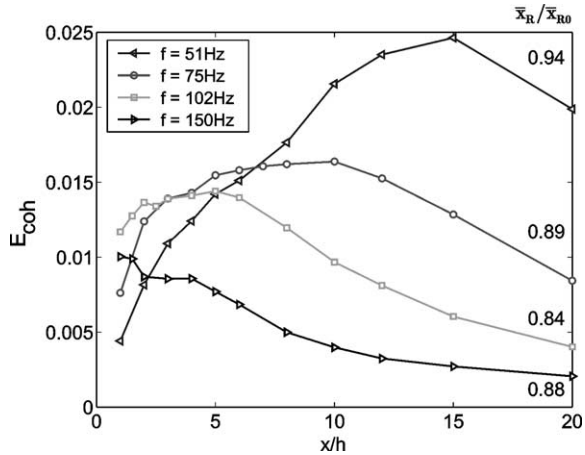

Fig. 12. Development of the coherent kinetic energy $E_{\mathrm{coh}}(u)$ at 4 excitation frequencies for $A = 25\%$, $\alpha = 20^\circ$ and $\mathrm{Re}_h = 5330$.

Fig. 12 presents the development of $E_{\mathrm{coh}}(u)$ in streamwise direction for $\alpha = 20^\circ$ and $A = 25\%$ at four excitation frequencies ($f = \{51, 75, 102, 150\}$ Hz) and a bandwidth of $\Delta f = 4$ Hz. This is an arbitrary choice of Δf but there is no change in the trend of E_{coh} if Δf is as large as 8 Hz. Amplification, saturation and a decrease of the coherent energy can be observed. Each curve has a saturation value $(E_{\mathrm{coh}})_{\max}$ at different height and at a different streamwise location x/h. This behavior is typical of a Kelvin–Helmholtz instability. A comparison of Figs. 12 and 10(a) shows that the largest reduction of the reverse-flow region ($\bar{x}_R/\bar{x}_{R0} = 0.84$) occurs at $f = 102$ Hz which is not the curve with the absolute maximum ($f = 51$ Hz) but the curve with the highest values of E_{coh} very close to the fence. Here the flow manipulation is most effective to reduce the reattachment length.

The manipulation of the coherent structures in the separated shear layer may be explained further by measurements of the phase-averaged vorticity and the streamlines. The vortex dynamics for case UF are presented in Fig. 13 where the vorticity component $\langle\omega_z\rangle = \partial\langle\bar{v}\rangle/\partial x - \partial\langle\bar{u}\rangle/\partial y$ is shown in the x, y-plane $-2 \leqslant x/h \leqslant 8$ and $0 \leqslant y/h \leqslant 3$ at four phase angles ϕ for the parameters: $A = 88\%$, $\mathrm{St}_h = 0.07$ and $\alpha = 20^\circ$. The streamlines are viewed from a coordinate system moving with the convection velocity of the structures $\bar{u}_c \approx 0.6U_N$ and the data were obtained by LDA. During the "suction" phase of the actuator (ϕ approximately between 30° and 150°) a structure (A) forms downstream of the tip of the fence. Subsequently during the "blowing" phase a structure (B) is generated in front of the fence, the angle of the streamlines at the fence tip changes and structure (A) is convected downstream. This strong excitation produces a periodical incoming flow which generates vortices similar to those in a starting flow. Therefore these vortices are also denominated as "starting" vortices.

For case TF and single frequency excitation ($A = 25\%$, $\mathrm{St}_h = 0.128$, $\mathrm{St}_{\delta_2} = 0.018$ and $\alpha = 20^\circ$) PIV measurements were made (not shown here). They show the expected roll-up of the shear-layer to a large coherent structure just downstream of the fence (not shown here). No vortex pairing could be observed in the instantaneous vorticity fields.

4.2. Bimodal forcing

Many investigations of free shear layers have shown that the control range of forcing can be increased by adding the excitation of the first subharmonic frequency $f_{\mathrm{sub}} = \frac{1}{2}f$ (e.g., Husain and Hussain [22] or König [23]). The disturbance signal is then described by

$$\mathrm{Signal} = A_{\mathrm{fun}}\sin(2\pi f t) + A_{\mathrm{sub}}\sin(2\pi f/2t + \Delta\varphi) \quad \text{with } 0^\circ \leqslant \Delta\varphi < 180^\circ.$$

For a bimodal excitation we need the amplitudes and the frequencies of the fundamental and the subharmonic excitation as well as the optimum initial phase difference $\Delta\varphi$. The aim of bimodal forcing is to maximize the subharmonic growth by tuning the initial phase difference (subharmonic resonance). $\Delta\varphi_{\mathrm{opt}}$ was determined for the parameter combination $A_{\mathrm{fun}} = A_{\mathrm{sub}} = 25\%$ (i.e., $A_{\mathrm{tot}} = 35\%$) and $f_{\mathrm{fun}} = 102$ Hz (cf. Fig. 10(a)) with $f_{\mathrm{sub}} = 51$ Hz from hot-wire measurements in the outer part of the shear layer at $x/h = 10$. Fig. 14 shows that A_{fun} is approximately independent of $\Delta\varphi$ but slightly lower than A_{fun} for single frequency excitation, whereas A_{sub} increases steeply beyond $\Delta\varphi = 20^\circ$ until a maximum is reached, here at $\Delta\varphi_{\mathrm{opt}} = 100^\circ$. The same trend can be seen from the distribution of $E_{\mathrm{coh}}(u)$ in x-direction (Fig. 15), i.e., a strong amplification of the first subharmonic component at $\Delta\varphi_{\mathrm{opt}} = 100^\circ$ and a weak one at $\Delta\varphi_{\mathrm{opt}} = 20^\circ$. For both cases the saturation of the first subharmonic does not occur near the fence. For an efficient reduction of the reattachment length energy containing structures, however,

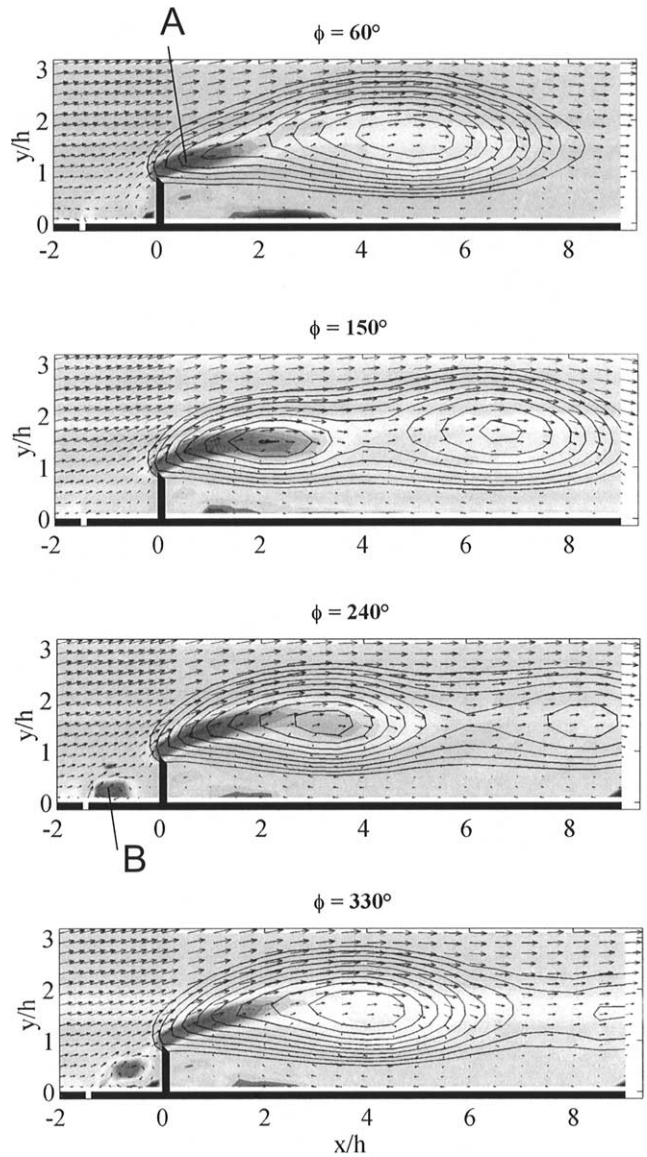

Fig. 13. Phase-averaged vorticity component $\langle\omega_z\rangle$ at $\mathrm{St}_h = 0.07$, $A = 88\%$, and $\alpha = 20°$ (excitation upstream of the fence) for four phase angles.

Table 1
Parameters of the single and bimodal excitations for $\mathrm{Re}_h = 5330$; $\alpha = 20°$; $B/h = 50$; $h/H = 2.4\%$; $\delta/h \approx 2$ and $x_{R0}/h = 15.0$

Excitation	Symbol	f_{fun} [Hz]	f_{sub} [Hz]	A_{fun} [%]	A_{sub} [%]	A_{tot} [%]	$\Delta\varphi$ [°]	$\bar{x}_R/\bar{x}_{R0}$ [1]	$\mathrm{St}_h(f_{\mathrm{fun}})$ [1]	$\mathrm{St}_{\delta_2}(f_{\mathrm{fun}})$ [1]
none	○	–	–	–	–	–	–	1	–	–
UF	□	55	–	88	–	88	–	0.67	0.07	0.010
TF	◇	102	–	25	–	25	–	0.84	0.128	0.018
TF	not shown	102	–	35	–	35	–	0.81	0.128	0.018
TF	△	102	–	88	–	88	–	0.65	0.128	0.018
TF	not shown	102	51	25	25	35	100	0.81	0.128	0.018
TF	not shown	102	51	25	25	35	20	0.83	0.128	0.018
TF	▽	204	102	25	25	35	80	0.75	0.255	0.036
TF	◁	204	102	25	25	35	20	0.88	0.255	0.036

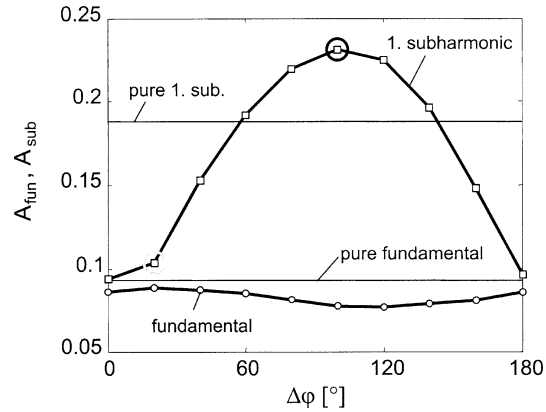

Fig. 14. Harmonic and subharmonic wave amplitude A_{fun} and A_{sub} as a function of the initial phase difference $\Delta\varphi$ for $f_i = \{51, 102\}$ Hz at $x/h = 10$.

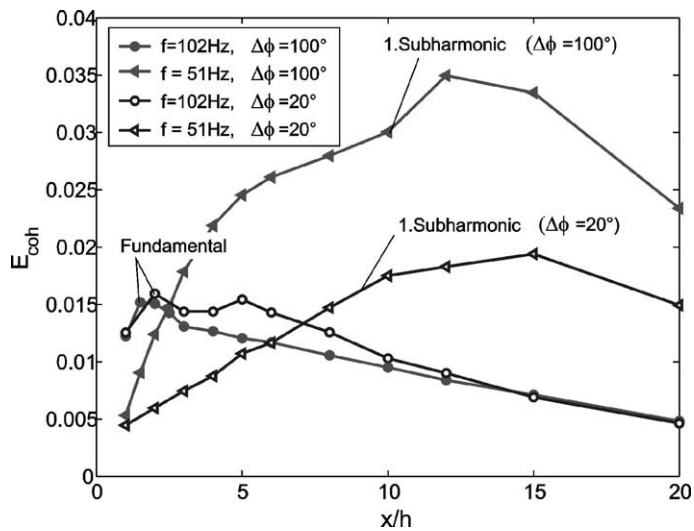

Fig. 15. Development of the integral coherent energy $E_{\text{coh}}(u)$ in x-direction at $f_i = \{51, 102\}$ Hz and $\Delta\varphi_i = \{20°, 100°\}$.

must be generated further upstream (see also Sigurdson and Roshko [24]). This can be achieved by choosing $f_{\text{fun}} = 204$ Hz, $f_{\text{sub}} = 102$ Hz and $\Delta\varphi_{\text{opt}} = 80°$ (the optimum for this combination of excitation frequencies).

The result of this manipulation is presented in Fig. 16 where the phase averaged vorticity $\langle\omega_z\rangle$ is plotted for four phase angles. The data were obtained from PIV measurements using 100 realizations for each phase angle. It shows the rolling up of two small vortices (A) and (B) which amalgamate to a bigger one (C) at $x/h \approx 5$. This forced vortex pairing leads to a reduction of $\bar{x}_R/\bar{x}_{R0}$ of 25%. The results and the respective parameters of the single and bimodal excitations are summarized in Table 1.

5. Discussion of wall data, mean velocity and Reynolds-stress profiles

5.1. Measurements on the wall

Measurements on the wall are presented as distributions along a line through $z/h = 16.6$ in the homogeneous region downstream of the swept fence ($\alpha = 20°$). They are the pressure coefficient $c_p = (p - p_{\text{ref}})/(0.5\rho U_N^2)$, the mean and fluctuating skin-friction coefficients $c_{fx} = \tau_{wx}/(0.5\rho U_N^2)$ and $c'_{fx} = \tau'_{wx}/(0.5\rho U_N^2)$ and the reverse-flow parameter χ_w. The data were plotted against x/h because the effects of the manipulation are easily recognized and the two other scaling parameters $x/\bar{x}_R$

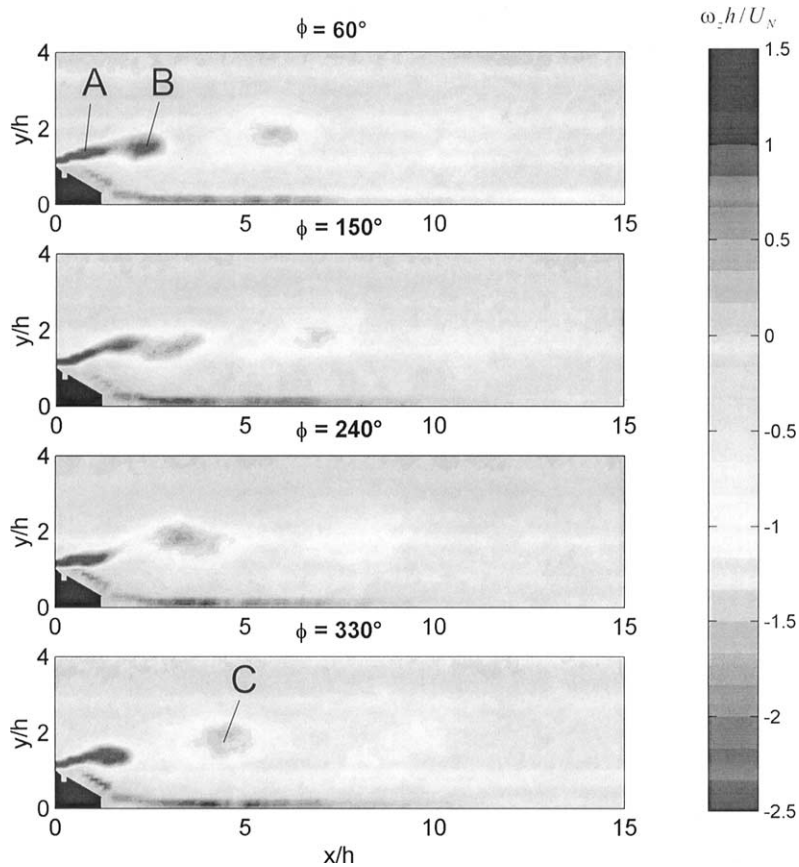

Fig. 16. Distributions of the phase-averaged vorticity component $\langle\omega_z\rangle$ for bimodal excitation ($f_i = \{204, 102\}$ Hz, $\Delta\varphi = 80°$, subharmonic resonance) at four phase angles.

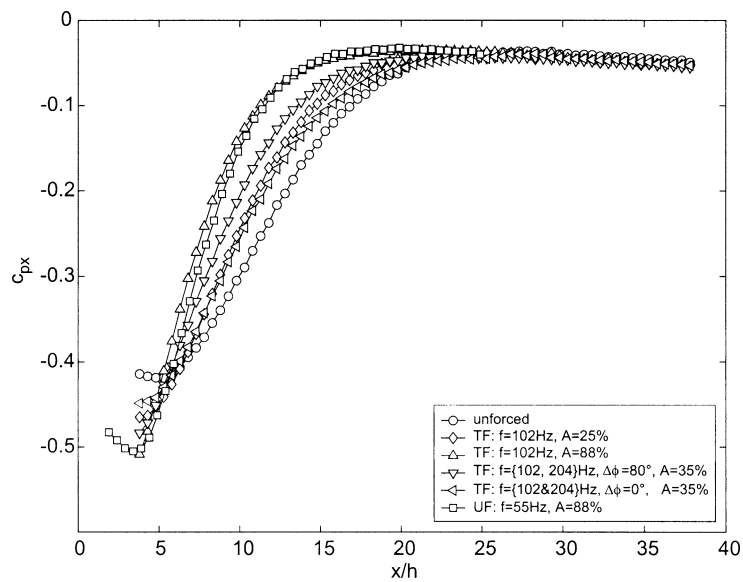

Fig. 17. Wall pressure distributions downstream of the fence with and without forcing.

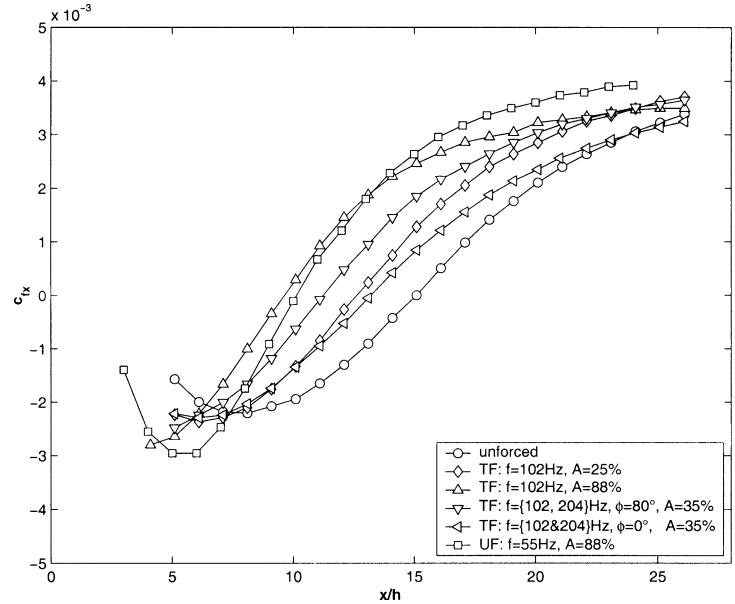

Fig. 18. Distributions of the mean skin friction coefficient downstream of the fence with and without forcing.

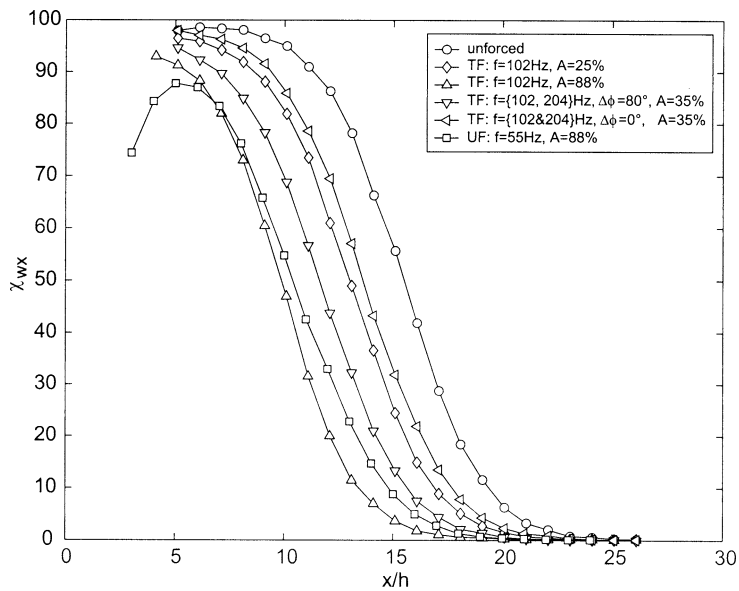

Fig. 19. Distributions of the reverse-flow factor χ_w downstream of the fence with and without forcing.

and $(x - \bar{x}_R)/h$ do not lead to more general conclusions ($\bar{x}_R$ is the mean position of the reattachment line). The distribution of the wall parameters have in common that the unforced case ($\circ$) and the manipulated cases with the highest amplitude $A = 88\%$ ($\triangle, \square$) denote the limits of the manipulation process. The reduction of the reattachment length is accompanied by a larger curvature of the streamlines resulting in a lower negative pressure coefficient c_p in the vicinity downstream of the fence. Since all c_p curves collapse onto each other downstream of reattachment (Fig. 17) the overall pressure recovery is not changed. Fig. 18 shows the respective skin friction distributions which are characteristic of a "strong reverse-flow region" (Fernholz [25]). The limit of the upstream movement of the reattachment line ($c_{fx} = 0$) due to the manipulation is clearly visible and the correlation between $c_{fx} = 0$ and $\chi_w = 50\%$ (Fig. 19) is confirmed (e.g., Dengel and Fernholz [26]). χ_w for the case with upstream

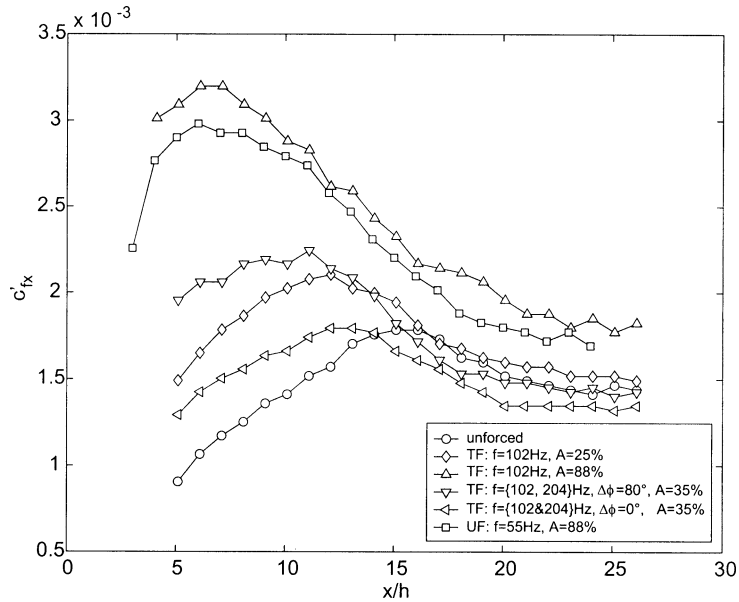

Fig. 20. Distributions of the fluctuating skin-friction coefficient downstream of the fence with and without forcing.

manipulation (UF) has a maximum value of 88% compared with 98% without manipulation and falls steeply in the direction of the fence. This indicates the existence of a pronounced region of downstream flow very close to the fence as had also been observed by Ruderich and Fernholz [27]. Note that the region with instantaneous reverse flow extends about one bubble length downstream of reattachment. Strong effects of the manipulation manifest themselves in the distributions of c'_{fx} (Fig. 20). Whereas the position of the respective maximum lies slightly upstream of reattachment (e.g., Siller [3]), the magnitude of the maximum between cases without and with manipulation differs by about 100%, caused by the strong mixing effects of the coherent structures generated just downstream of the fence.

5.2. Mean velocity and Reynolds-stress profiles

Measurements of the mean velocity and Reynolds-stress profiles were made at positions $0 \leqslant x/h \leqslant 16$ downstream of the fence by means of LDA. From among the many profiles two case studies were selected: (1) no manipulation and (2) optimum manipulation ($A = 88\%$) upstream of the fence (UF). Figs. 21 and 22 present the profiles of the three components of the mean velocity and of four Reynolds stresses for the cases without and with manipulation (UF) extending from the wall to five fence heights. The streamwise profiles $\bar{u}/U_N$ show both the development of the separated shear layer and the reverse-flow region with maximum values of the mean reverse-flow velocity $|\bar{u}/U_N| = 0.35$ and 0.25 for the forced and unforced flow, respectively. The locus $\bar{u} = 0$ remains below $y/h = 1$ in both cases, except very close to the fence.

The magnitude of $\overline{w}$ is increased by the manipulation and $\overline{w}/U_N$ has maximum values of about 0.38. The $\overline{w}$ profiles show a local minimum as was observed in the flow downstream of a swept backward-facing step (Kaltenbach and Janke [9]) and the near-wall maximum grows in streamwise direction.

The profiles of $\bar{v}$ show positive values to about $x/h = 4$ and, very close to the fence, $\bar{v}/U_N$ is of the order of one. At $x/h = 6$, $\bar{v}$ remains approximately zero below $y/h = 2$ for case 1 and negative for the case with forcing which shows the increased flow towards the wall. The magnitude of $\bar{v}$ decreases in downstream direction for both cases.

Although the mean velocity profiles are clearly affected by the manipulation, the effect is still stronger on the turbulence structure in the reverse-flow region and, as far as $\overline{u'^2}$ is concerned, deep into the relaxation region downstream. As is characteristic of separated shear layers the maxima of the Reynolds stresses go together with the maximum of the mean shear shear $\partial\bar{u}/\partial y$. For $\overline{u'^2}$, $\overline{v'^2}$ and $\overline{u'v'}$ the distance of their maximum above the wall increases until a maximum value is reached at about $x/h = 6$ and remains approximately constant downstream. The development of $\overline{w'^2}$ differs from that of $\overline{u'^2}$ and $\overline{v'^2}$ in that firstly its maximum moves from the shear layer towards the wall with increasing distance from the fence and secondly the influence of the large-scale structures affects the region below $y/h = 1.5$.

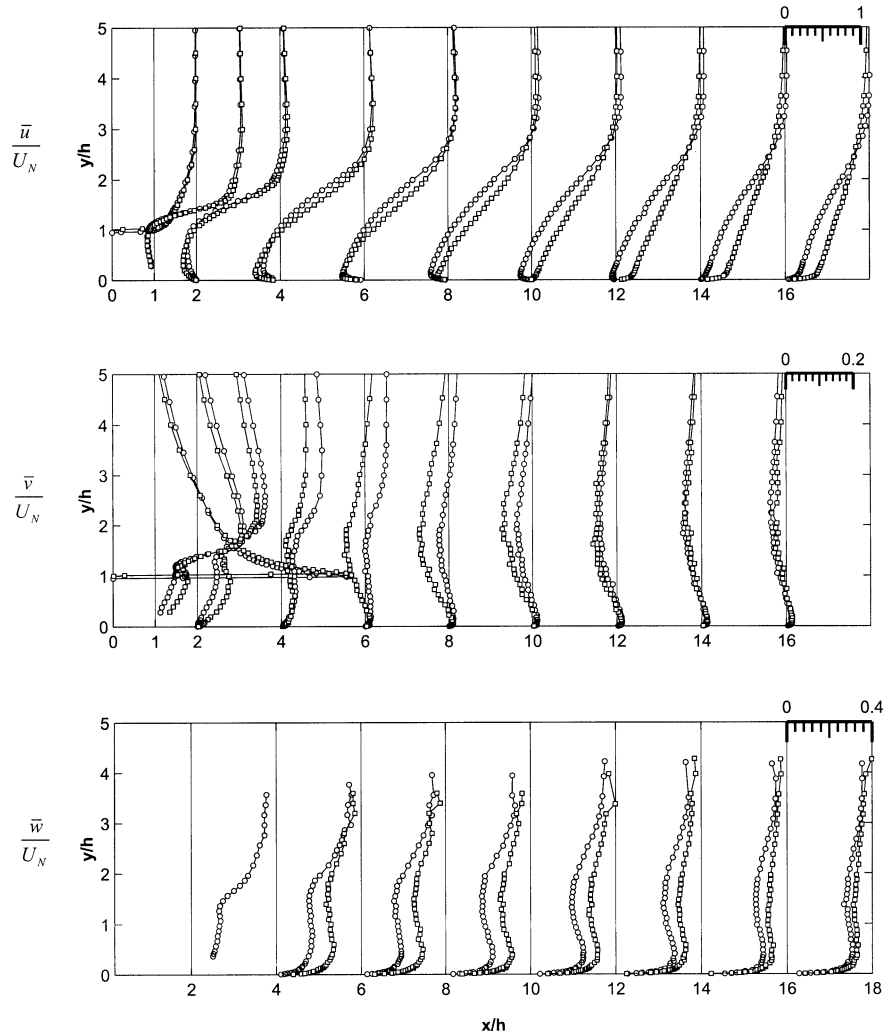

Fig. 21. Mean velocity profiles downstream of the fence for the case without and with manipulation (UF).

The Reynolds stresses can now be used to show the distribution of the integrated values of the turbulent energy and the integrated turbulence production in x-direction for the cases with (UF) and without manipulation. If the non-dimensional Reynolds normal stresses $\overline{u'^2}$ and $\overline{v'^2}$ are integrated from the wall to the edge of the shear layer the following integrals result

$$E\left(\overline{u'^2}\right) = \int_0^\infty \frac{\overline{u'^2}}{U_N^2}\,\mathrm{d}(y/h) \quad \text{and} \quad E\left(\overline{v'^2}\right) = \int_0^\infty \frac{\overline{v'^2}}{U_N^2}\,\mathrm{d}(y/h).$$

These integrals are plotted against x/h in Fig. 23 and show a strong increase downstream of the fence reaching a maximum just downstream of the respective reattachment region. With manipulation the maxima are higher in agreement with Fig. 22 and with the the production maxima for $\overline{u'^2}$. The maxima are situated in the shear layer above the closed reverse-flow region where the product of $\overline{u'v'}$ and $\partial\bar{u}/\partial y$ is largest. The dimensionless integral value of the production term for $\overline{u'^2}$,

$$P\left(\overline{u'^2}\right) = \int_0^\infty \frac{\overline{u'v'}}{U_N^3}\frac{\partial\bar{u}}{\partial y}\,\mathrm{d}y,$$

was calculated for sweep angles $\alpha = 0°$ and $20°$ with and without manipulation for case UF and is shown in Fig. 24. Without manipulation the production is slightly higher for the swept flow than for the unswept one in accordance with a slightly smaller

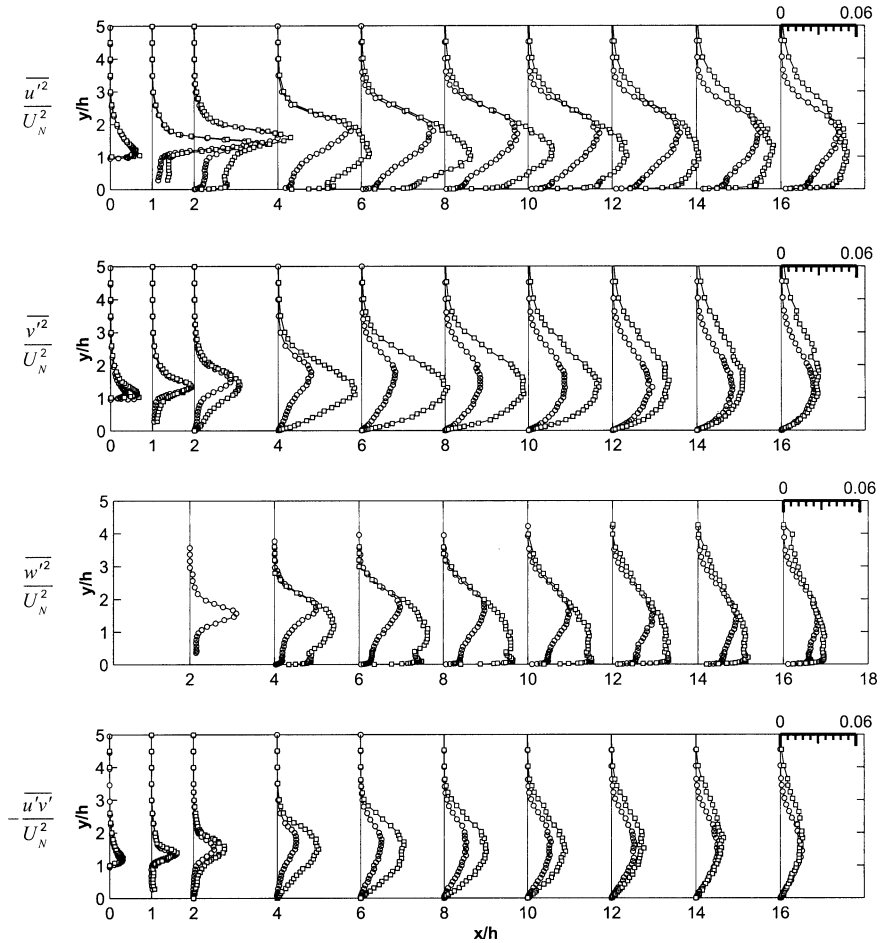

Fig. 22. Profiles of 4 Reynolds stresses downstream of the fence for the case without and with manipulation (UF).

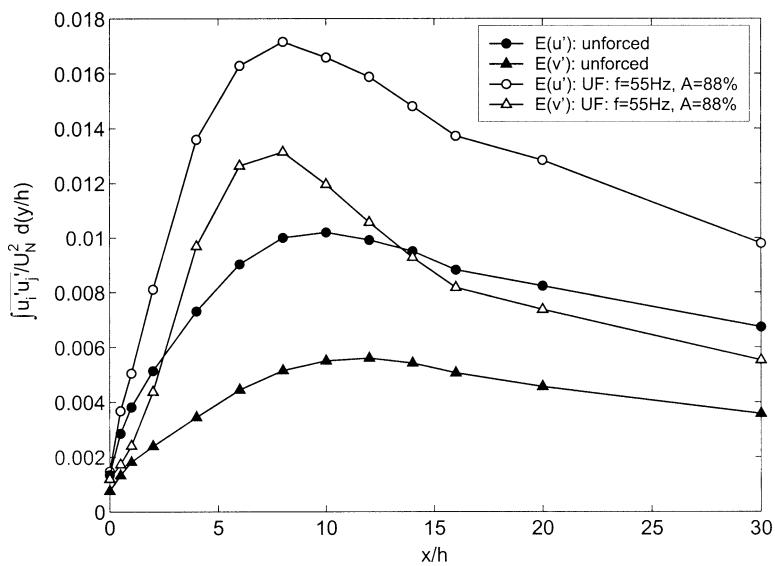

Fig. 23. Development of the integral kinetic energy in x-direction for the case without and with manipulation (UF).

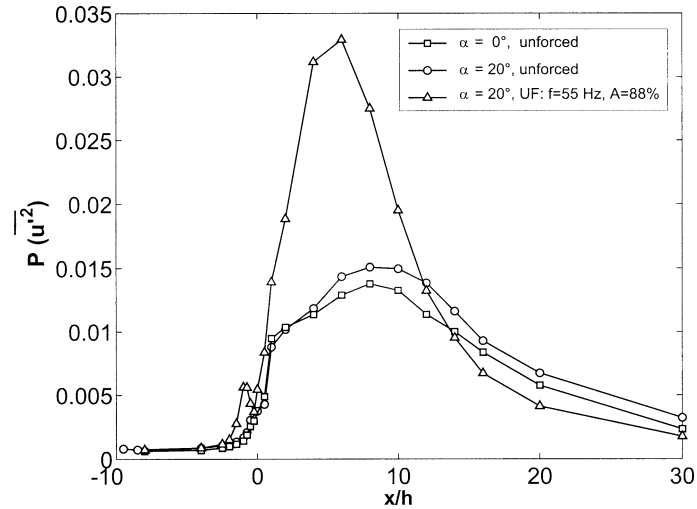

Fig. 24. Development of the integral turbulence production of u in x-direction for the case without and with manipulation (UF).

reattachment length. With manipulation the maximum value of the production of the turbulent kinetic energy is increased by about 150%. This reduces the reattachment length by large-scale mixing but increases the loss of energy of the mean motion at the same time. The maximum of $P(\overline{u'^2})$ lies approximately in the middle of the reverse-flow region and then falls sharply to very low values downstream.

6. Conclusions

Owing to the two separation regions of this flow configurations, the flow could be influenced both at the separation line upstream of the fence or at the fixed separation line at the tip of the fence. Using a loudspeaker-slot actuator which introduced an oscillating jet, Strouhal number, amplitude parameter and phase angle were optimized to obtain a maximum reduction of the reattachment length downstream of the fence. The experimental results for the parameter range given above allow the following conclusions:

- For a high amplitude of $A \equiv v'/U_N = 88\%$ the largest reduction of the reverse-flow region length is practically independent of the excitation mechanism – generation of a starting vortex at the fence or vortex excitation by the Kelvin–Helmholtz instability close to the fence. For low amplitudes only the excitation of the Kelvin–Helmholtz instability shortens the separation bubble.
- Bimodal excitation of the Kelvin–Helmholtz instability at the optimum phase difference (subharmonic resonance) is only slightly more effective than single mode excitation at the same total forcing amplitude.
- In accordance with Sigurdson and Roshko [24] the growth rate of the coherent structures will depend on how well the excitation is amplified and where the amplification occurs.
- The large coherent structures, responsible for entrainment and thus for the reduction of the reattachment length must be generated as closely to the fence, i.e. to separation, as possible.
- Figures 13 and 16 show that the structures generated by the roll-up of the shear layer lose their intensity over a short distance downstream and are no longer visible in the reattachment region. This is supported by the fast decrease of the coherent energy $E_{\mathrm{coh}}(u)$ (see Figs. 12 and 15).

The manipulation increases the Reynolds stresses in the reverse-flow region and the mean reverse-flow velocity component $\bar{u}$ as well as $\overline{w}$ in spanwise direction.

Acknowledgements

A. Huppertz is grateful for the financial support by DFG within the framework of Sfb 557. We thank S. Reitebuch who assisted with the measurements.

References

[1] P. Bradshaw, F.Y.F. Wong, The reattachment and relaxation of a turbulent shear layer, J. Fluid Mech. 52 (1972) 113–135.
[2] H.A. Siller, H.H. Fernholz, Control of separated flow downstream of a two-dimensional fence by low-frequency forcing, Appl. Sci. Res. 57 (1997) 309–318.
[3] H.A. Siller, Reduction of the recirculation length downstream of a fence by an oscillating cross flow, Dissertation, Technische Universität Berlin, 1999.
[4] A. Huppertz, Aktive Beeinflussung der Strömung stromab einer rückwärtsgewandten Stufe, Dissertation, Technische Universität Berlin, 2001, http://edocs.tu-berlin.de/diss/2001/.
[5] M.A.Z. Hasan, The flow over a backward-facing step under controlled pertubation: laminar separation, J. Fluid Mech. 238 (1992) 73–96.
[6] H.H. Fernholz, G. Janke, M. Kalter, M. Schober, On the separated flow behind a swept backward-facing step, in: K. Gersten (Ed.), Physics of Separated Flows – Numerical, Experimental & Theoretical Aspects, Vieweg, 1993, pp. 200–207.
[7] K.B. Chun, H.J. Sung, Control of turbulent separated flow over a backward-facing step by local forcing, Exp. in Fluids 21 (1996) 417–426.
[8] A. Huppertz, G. Janke, Preliminary experiments on the control of three-dimensional modes in the flow over a backward-facing step, in: S. Gavrilakis, L. Machiels, P.A. Monkewitz (Eds.), Advances in Turbulence, Vol. VI, Kluwer, 1996, pp. 461–464.
[9] H. Kaltenbach, G. Janke, Direct numerical simulation of flow separation behind a swept, rearward-facing step at $\mathrm{Re} = 3000$, Phys. Fluids 12 (2000) 2320–2337.
[10] H. Wengle, A. Huppertz, G. Bärwolff, G. Janke, The manipulated transitional backward-facing step flow: an experimental and direct numerical simulation investigation, Eur. J. Mech. B/Fluids 20 (2001) 25–46.
[11] P.E. Hancock, F.M. Mc Cluskey, Spanwise invariant three-dimensional separated flow, J. Exp. Thermal Fluid Sci. 14 (1997) 25–34.
[12] J.R. Hardman, P.E. Hancock, Measurements in a three-dimensional separation, in: S. Gavrilakis, L. Machiels, P.A. Monkewitz (Eds.), Advances in Turbulence, Vol. VI, Kluwer, 1996, pp. 453–456.
[13] J.R. Hardman, P.E. Hancock, The near-wall layer beneath a moderately converging three-dimensional turbulent separated and reattaching, Eur. J. Mech. B/Fluids 19 (2000) 653–672.
[14] M. Schober, Beeinflussung inkompressibler turbulenter Wandstrahlen, Dissertation, Technische Universität Berlin, 1999.
[15] P. Dengel, Über die Struktur und Sensibilität einer inkompressiblen turbulenten Grenzschicht am Rande der Ablösung, Dissertation, Technische Universität Berlin, 1992.
[16] R.D. Kean, R.J. Adrian, Theory of cross-correlation analysis of PIV images, Appl. Sci. Res. 49 (1992) 191–215.
[17] H.H. Fernholz, G. Janke, M. Schober, P.M. Wagner, D. Warnack, New developments and applications of skin-friction measuring techniques, Meas. Sci. Technol. 7 (1996) 1396–1409.
[18] H. Bippes, Basic experiments on transition in three-dimensional boundary layer dominated by crossflow instability, Prog. Aerosp. Sci. 35 (1999) 363–412.
[19] P.R. Spalart, Direct simulation of a turbulent boundary layer up to $\mathrm{Re}_\theta = 1410$, J. Fluid Mech. 187 (1988) 61–98.
[20] C.M. Ho, P. Huerre, Perturbed free shear layers, Annu. Rev. Fluid Mech. 16 (1984) 365–424.
[21] C.M. Ho, L.S. Huang, Subharmonics and vortex merging in mixing layers, J. Fluid Mech. 119 (1982) 443–473.
[22] H. Husain, A.K. Hussain, Experiments on subharmonic resonance in a shear layer, J. Fluid Mech. 304 (1995) 343–372.
[23] O. König, Untersuchungen an einer verzögerten Scherschicht, Dissertation, Technische Universität Berlin, 1997.
[24] L.W. Sigurdson, A. Roshko, The structure and control of a turbulent reattaching flow, in: H.W. Liepmann, R. Narasimha (Eds.), IUTAM Symp. Turbulence Management and Relaminarization, Springer-Verlag, 1988, pp. 914–919.
[25] H.H. Fernholz, Near-wall phenomena in turbulent separated flows, Acta Mech. 4 (1994) 57–67.
[26] P. Dengel, H.H. Fernholz, An experimental investigation of an incompressible turbulent boundary layer in the vincinity of separation, J. Fluid Mech. 212 (1990) 615–636.
[27] R. Ruderich, H.H. Fernholz, An experimental investigation of the structure of a turbulent shear flow with separation, reverse flow, and reattachment, J. Fluid Mech. 163 (1986) 283–322.